Analytical Biochemistry 705 (2025) 115924

Contents lists available at ScienceDirect

Analytical Biochemistry

journal homepage: www.elsevier.com/locate/yabio

A proof-of-concept diagnostic platform for neonatal calf diarrhea using serum infrared spectroscopy and predictive analytics

Nuri Ceran [a], Rafig Gurbanov [b,c,*]

[a] Department of Bioengineering, Institute of Graduate Studies, Bilecik Şeyh Edebali University, Bilecik, 1100, Türkiye
[b] Department of Bioengineering, Bilecik Şeyh Edebali University, Bilecik, 1100, Türkiye
[c] Central Research Laboratory, Bilecik Şeyh Edebali University, Bilecik, 1100, Türkiye

ARTICLE INFO

Keywords:
Neonatal calf diarrhea
Infrared spectroscopy
Predictive analytics
Machine learning
Spectrochemical index
Non-invasive diagnosis

ABSTRACT

This study presents a novel diagnostic platform for the rapid and non-invasive detection of neonatal calf diarrhea using ATR-FTIR spectroscopy combined with predictive analytics. Neonatal calf diarrhea is a leading cause of economic losses and animal welfare issues in the cattle industry, and current diagnostic methods are often time-consuming and require invasive sampling. Our approach leverages the unique biochemical fingerprints of serum obtained from healthy, diseased, and recovered calves. The spectral data were preprocessed and analyzed using Principal Component Analysis to extract key molecular features, which were subsequently classified using Linear Discriminant Analysis and Support Vector Machines. These predictive models demonstrated high accuracy in distinguishing the physiological states of the calves, underscoring the potential of this platform as a reliable diagnostic tool. Another significant innovation of this work is the development of the 1080 cm^{-1}/3300 cm^{-1} spectrochemical index, a single, interpretable parameter derived from the ratio of the PO_2^- symmetric stretching band to the Amide A band. This quantitative index correlates with molecular-level changes associated with disease progression and recovery, further enhancing diagnostic precision and enabling timely intervention. The integration of spectral data into an easily interpretable metric contributes to improved animal welfare and sustainable livestock management practices.

1. Introduction

Neonatal calf diarrhea (NCD), also known as calf scours, is a commonly reported disease in young calves and remains a major cause of economic losses for cattle producers worldwide [1]. Diarrhea can result in decreased short- and long-term productivity. Calf diarrhea is a multifactorial disease stemming from the interactions between infectious agents, the environment, and the calf itself [1,2]. Many factors influence calf diarrhea outbreaks, broadly categorized as agent factors, host susceptibility, and environmental conditions [3]. Disease occurs when the calf's defenses are overwhelmed, generally because of a combination of factors. A single primary pathogen can cause calf diarrhea, but co-infection is frequently observed in diarrheic calves. An effective contact is exposure to pathogens of a dose load or duration sufficient to cause disease [3]. Multiple factors, both infectious and non-infectious, are involved in calf diarrhea outbreaks, which makes disease control on farms [4]. Multiple enteric pathogens like viruses, bacteria, and protozoa are often involved, with co-infection being frequently observed. The prevalence of each pathogen and disease incidence can vary based on geographic location, farm management practices, and herd size [5]. Non-infectious factors include insufficient colostrum intake, poor sanitation, stress, overcrowding, and cold weather [2].

NCD is a major cause of calf mortality, accounting for over 50 % of deaths, and leads to significant economic losses in the cattle industry, with costs varying by region and pathogen [6–8]. Its prevalence ranges from 23 % in Canada to 58 % in Iran, with causative agents including bovine rotavirus, coronavirus, *Escherichia coli*, *Salmonella*, *Clostridium perfringens*, and *Cryptosporidium parvum*. However, these pathogens can also be found in healthy calves, highlighting the multifactorial nature of the disease. The gastrointestinal microbiota plays a critical role in calf health by supporting nutrient absorption, immune regulation, and intestinal development. Dysbiosis, or microbial imbalance, is linked to gastrointestinal disease, though it remains unclear whether it precedes or follows pathogen invasion [9,10]. Effective management hinges on early diagnosis via fecal antigen testing and prompt fluid therapy to

* Corresponding author. Department of Bioengineering, Bilecik Şeyh Edebali University, Bilecik, 1100, Türkiye.
E-mail address: rafig.gurbanov@bilecik.edu.tr (R. Gurbanov).

https://doi.org/10.1016/j.ab.2025.115924
Received 13 March 2025; Received in revised form 11 June 2025; Accepted 12 June 2025
Available online 14 June 2025

correct electrolyte imbalances, alongside targeted antimicrobial use for bacterial coinfections [7]. Prevention strategies emphasize optimizing colostral IgG transfer, dam vaccination to enhance passive immunity, and rigorous biosecurity to limit environmental pathogen loads [11]. Despite advances, NCD remains economically devastating, underscoring the need for integrated herd health programs to mitigate losses [12].

Most diarrhea in young calves are treated with antimicrobials. However, excessive antimicrobial usage can lead to antimicrobial resistance and can negatively impact the gut microflora of a calf. Certain pathogens associated with calf diarrhea can be harmful to human health due to their zoonotic potential and their ability to develop antimicrobial resistance, which can be passed on when meat and milk are consumed [13]. Treating NCD requires a multifaceted approach, starting with fluid therapy using oral or intravenous electrolyte solutions to correct dehydration and electrolyte imbalances [14,15]. When selecting an electrolyte, make sure it contains 100–120 mmol/L of sodium and 50–80 mmol/L of acetate or propionate. Antimicrobials such as ceftiofur or amoxicillin-clavulanate may be necessary for bacterial infections but should be used judiciously. Halofuginone lactate can be used to address *Cryptosporidium* infections [16]. Bovine colostrum, rich in bioactive factors, can serve as a therapeutic alternative to antimicrobials [13]. Nutritional management, involving a return to whole milk feeding and supplementation of colostrum, is also important. Additionally, prebiotics, probiotics, synbiotics, and fecal microbiota transplantation (FMT) can help restore gut health [8]. Oral administration of selected *Lactobacillus reuteri* isolates significantly reduced NCD, highlighting its promise as a probiotic [17]. Further refinements in application timing and strain selection could enhance its protective effects. Supportive care includes early identification, isolation of sick calves, maintaining hygiene, and providing a dry, warm environment [2]. The European Food Safety Authority (EFSA) emphasizes transitioning to group housing, improving dietary practices, and ensuring cow-calf bonding to enhance calf welfare. Legislative updates should prioritize space, social contact, and fiber/iron provision, particularly in veal systems [18].

Laboratory testing is needed for an accurate diagnosis of calf diarrhea because various pathogens or factors can be involved in the disease's development. A quick diagnosis is critical to confirm the cause and implement appropriate interventions. Diagnostic outcomes can be influenced by sampling time and population, specimen quality, and laboratory methods. Fecal samples are commonly examined via microscopy, bacterial culturing, and PCR. Intestinal tissues are tested using immunohistochemistry or bacterial culturing. Rapid detection methods, such as PCR, RT-PCR, and Ag-ELISA, are commonly used to identify pathogens in clinical specimens. Clinicians should consider farm and clinical history together with lab results to identify the causative pathogen [5,19]. When the cause of diarrhea is unknown, electron microscopy (EM) can be used [20]. Several factors can impact diagnostic outcomes. Pathogen isolation can be difficult in the gastrointestinal environment [21]. Direct EM is not a specific test and has low sensitivity. It also requires many viral particles for virus detection and cannot concurrently evaluate multiple samples. The cost of EMs and the requirement of skilled personnel can also be a challenge for routine diagnostic testing. The analytic sensitivity of Ag-ELISA tends to be lower than isolation/culture or nucleic-acid-based assays, and the cost of commercial kits may be cost-prohibitive. Bacterial culture can take 24–72 h, and turnaround time can vary depending on culture methods and diagnostic instrumentation. Immunological or nucleic acid-based assays may be required for bacterial identification [5,22]. Molecular diagnostics such as PCR, metabolomics profiling, or volatile compound biomarker analysis are not feasible for in-field or real-time applications due to substantial sample purification and preparation, specialized facilities, special handling, storage, and transport of biological samples, increasing the risk of contamination and degradation [23].

Recent study investigated the use of Near Infrared Spectroscopy (NIRS) combined with multivariate analysis (MVA) to diagnose and monitor *Mannheimia haemolytica* infection in dairy calves, a major cause of bovine respiratory disease (BRD). The performance of NIRS was comparable to other diagnostic techniques such as ELISA, PCR, and NMR, but with the added advantages of being rapid, portable, and requiring minimal sample preparation [23]. Another study evaluated and compared the performance of infrared (IR) spectroscopy for the rapid measurement of bovine serum immunoglobulin G (IgG) concentration and detection of failure of transfer of passive immunity (FTPI) in dairy calves. It was concluded that IR spectroscopic technique combined with multivariate analysis is effective for quantifying IgG levels and diagnosing FTPI in dairy calves, with ATR-IR being particularly advantageous for field applications [24]. A very recent study demonstrated the feasibility of using FTIR spectroscopy combined with machine learning (ML) as a rapid and effective screening tool for identifying multidrug-resistant *E. coli* strains in calves, with potential applications in microbiology laboratories and livestock management [25]. The previous study demonstrated that NMR-based metabolomics can distinguish between healthy calves and those with diarrhea-induced sepsis, providing insights into the pathogenesis of sepsis in calves and identifying novel biomarkers for early diagnosis and prognosis [26].

To the best of our knowledge, there is currently no comprehensive study addressing the rapid, cost-effective, and non-invasive diagnosis of NCD through the analysis of serum biomolecules, irrespective of the underlying infectious agent. This gap in research highlights the critical need for innovative methodologies that prioritize early detection, differential diagnosis, and pathogen-agnostic screening to mitigate the economic losses in livestock production, improve animal welfare, and reduce the risk of zoonotic transmission. By leveraging advancements in analytical and predictive learning technologies, this proof-of-concept study aims to develop a cost-effective and relatively simple diagnostic framework capable of identifying diarrhea in calves without prior knowledge of specific pathogens. Thus, IR spectroscopy combined with supervised classification tools - Linear Discriminant Analysis (LDA) and Support Vector Machine (SVM) are used to construct a high-capable platform for the diagnosis of NCD from calf sera. Such an approach would not only enhance on-farm decision-making for timely therapeutic intervention but also provide a scalable and cost-effective tool for large-scale herd health monitoring, ultimately supporting sustainable agricultural practices and global food security.

2. Materials and methods

2.1. Animal grouping, whole blood sampling, and serum separation procedures

The study was conducted between January and May 2021 using blood samples collected from neonatal calves aged 1–20 days. The calves were divided into three distinct groups: healthy (H), diseased (D), and recovered (R). The protocol was approved by the Local Animal Experiments Ethics Committee of Niğde Ömer Halis Demir University (Approval No: E−86837521-050.99-257260). The study included Holstein breed calves raised on farms in Çavdarlı village, Niğde province. From each animal, a veterinarian collected blood into two biochemistry tubes. Individuals exhibiting diseases other than diarrhea were excluded. Blood samples from 10 individuals per group (totaling 30 samples, with two tubes per animal) were centrifuged at 3000 rpm for 15 min at +4 °C to separate serum from cellular components. Serum separation was performed at the Niğde Provincial Directorate of Agriculture and Forestry laboratory. Serum samples were transferred to 1 mL Eppendorf tubes, transported to the research laboratory at Bilecik Şeyh Edebali University on dry ice, and stored at −80 °C. Healthy calves without diarrhea were designated as control group.

2.2. ATR-FTIR spectroscopy of serum samples

Frozen serum samples were thawed at room temperature and vortexed prior to spectroscopic analysis. Without pretreatment, 1 μL of

serum was placed on the Zn/Se crystal of the ATR unit (PerkinElmer) and gently dried under a low-flow nitrogen stream for 2 min to remove unbound water. Spectra were acquired using an ATR-FTIR spectrometer (PerkinElmer) with optimized parameters (4 cm^{-1} resolution, 32 scans). Data collection was performed using Spectrum One software (PerkinElmer) across the 4000–650 cm^{-1} wavenumber range. Before each measurement, background air spectra were recorded. Triplicate measurements were taken for each sample, and their averages were used for subsequent analyses. Baseline correction was applied to average spectra for visual clarity, and preprocessing was conducted using OPUS 5.5 software (Bruker). Spectral biomarkers were identified through qualitative and quantitative analysis of integrated band areas and positional parameters using specialized software and methods [27–29]. In this, first the systematic inspection of the entire set of individual spectra across all experimental conditions was performed. This qualitative survey revealed that, in nearly every sample, the bands for PO_2^- symmetric stretch (~1080 cm^{-1}) and the Amide A NH stretch (~3300 cm^{-1}) exhibited the most consistent relative intensity changes between groups. Accordingly, the univariate and quantitative spectrochemical index was defined as the ratio of the integrated areas under these two bands (1080 cm^{-1}/3300 cm^{-1}) for each spectrum.

2.3. Predictive analytics

The Unscrambler® X 10.3 (CAMO Software AS) multivariate analysis (MVA) software was used for all predictive analytics. To develop a predictive model for diagnostic purposes; first, the IR datasets from calf sera (H, D, and R group datasets) were processed and subsequently analyzed using unsupervised and exploratory - principal component analysis (PCA) [30]. Raw spectral data within the 4000–650 cm^{-1} range underwent three preprocessing steps to minimize instrumentation-dependent biases in analyses. First, baseline correction was applied using an offset adjustment method using data columns 1–3351. Second, a Savitzky-Golay second-derivative transformation with a 9-point smoothing window was implemented to enhance spectral resolution using the same data columns. Third, unit-vector normalization was performed to standardize amplitude variations. The processed spectra were mean-centered and cross-validated via a 30-segment full method, utilizing a calibration set of 30 samples. PCA, executed through singular value decomposition (SVD), the matrix factorization algorithm, was independently applied to various spectral windows over the mid-IR region (4000–650 cm^{-1}). The model was constrained to 10 principal components (PCs) to optimize interpretability. The unsupervised method developed in this way was further analyzed using the supervised classification technique - Linear Discriminant Analysis (LDA) to develop a predictive model for disease diagnosis. LDA is a supervised classification method rooted in Bayes' theorem, distinguished by its simplicity among Bayesian classifiers. The technique aims to estimate model parameters that optimally separate classes by maximizing between-group variance relative to within-group variance. Once trained, the model assigns class labels to unobserved data points. LDA rests on two core assumptions: (1) each class-conditional distribution follows a multivariate normal distribution, and (2) all classes share identical covariance matrices (homoscedasticity). These assumptions collectively produce linear decision boundaries, making LDA computationally efficient and interpretable for classification tasks [31]. The category variable column was included in a data matrix, and then all spectra of different sample categories were used to generate a training set. Prior probabilities were calculated from the training set. The prediction model was constructed to project 10 PCs using the Mahalanobis method at different sub-regions of IR spectra. The results were visualized through discrimination plots, highlighting sample clustering, and prediction and confusion matrices, identifying each sample status/position in intergroup discrimination [32–34].

Support Vector Machine (SVM) is a supervised classification technique grounded in statistical learning theory, characterized by its ability to identify an optimal hyperplane that maximizes the margin between distinct classes. When linear separation is infeasible in the original feature space, SVM employs kernel functions to implicitly map data into a higher-dimensional space, where linear separation becomes viable. This "kernel trick" leverages dual representation, substituting explicit feature transformations with dot product computations, thereby enabling efficient handling of nonlinear relationships. Support vectors—the critical subset of training data closest to the decision boundary—define the hyperplane, ensuring computational efficiency. SVM offers distinct advantages, including a globally optimal solution due to its convex optimization framework, reduced risk of overfitting through margin maximization (a form of regularization), and adaptability to diverse data structures via kernel functions (e.g., polynomial, radial basis). Unlike neural networks, SVM's performance is less sensitive to parameter variations, and its reliance on quadratic programming ensures stable, reproducible results. These attributes make SVM particularly effective for complex, nonlinear classification tasks while maintaining computational tractability [31,35]. The classification model for the calf dataset was developed using SVM within the C–H stretching vibrational region (4000–2500 cm^{-1}) of the IR spectra. The SVM framework was configured with a nu-SVC (nu-Support Vector Classification, Classification SVM Type 2) algorithm, employing a linear kernel function and a nu parameter value of 0.5 to balance class separation and margin errors. Uniform class weights (1.00 for all classes) were applied to mitigate bias. Model robustness was ensured through 30-fold cross-validation, optimizing generalizability by iteratively partitioning the dataset into training and validation subsets.

2.4. Univariate statistical analyses

Univariate statistics were performed using GraphPad Prism 8.01 (GraphPad, USA). One-way ANOVA followed by Dunnett's test was used to assess significant differences between spectral parameters across groups. Significance levels were defined as $*p \leq 0.05$, $**p \leq 0.01$, $***p \leq 0.001$, and $****p \leq 0.0001$. Results are presented as bar graphs showing the mean ± standard error of the mean (SEM).

2.5. ROC analysis for discriminatory validation of spectral parameters

Receiver operating characteristic (ROC) analysis was performed using GraphPad Prism 8.01 to assess and validate the diagnostic efficacy of spectral band parameters in distinguishing between the two species. An optimal threshold was determined to maximize the differentiation of spectral profiles between groups. The resultant ROC curve delineated the relationship between sensitivity (true positive rate) and specificity (true negative rate) across incremental threshold values, providing a quantitative framework to evaluate classification performance. Sensitivity was defined as the proportion of correctly classified true positives, whereas specificity reflected the accuracy of true negative identification.

To quantify the overall diagnostic utility of the spectral parameters, the area under the curve (AUC) and its standard error (SE) were computed at a 95 % confidence interval. AUC values exceeding 0.5 were interpreted as indicative of discriminatory capacity, with higher values signifying enhanced discriminatory capacity. Only parameters yielding AUC values statistically greater than 0.5 ($p < 0.05$) were retained for further interpretation, ensuring analytical rigor [28].

3. Results

LDA results, illustrated in Fig. 1, present a discrimination plot differentiating serum of Healthy (H), Diseased (D), and Recovered (R) neonatal calves within the fingerprint region (1800–650 cm^{-1}) of the IR spectral data. The LDA model achieved perfect classification accuracy (100 %) in distinguishing all three groups, a performance consistently replicated across additional spectral sub-regions. This discriminatory

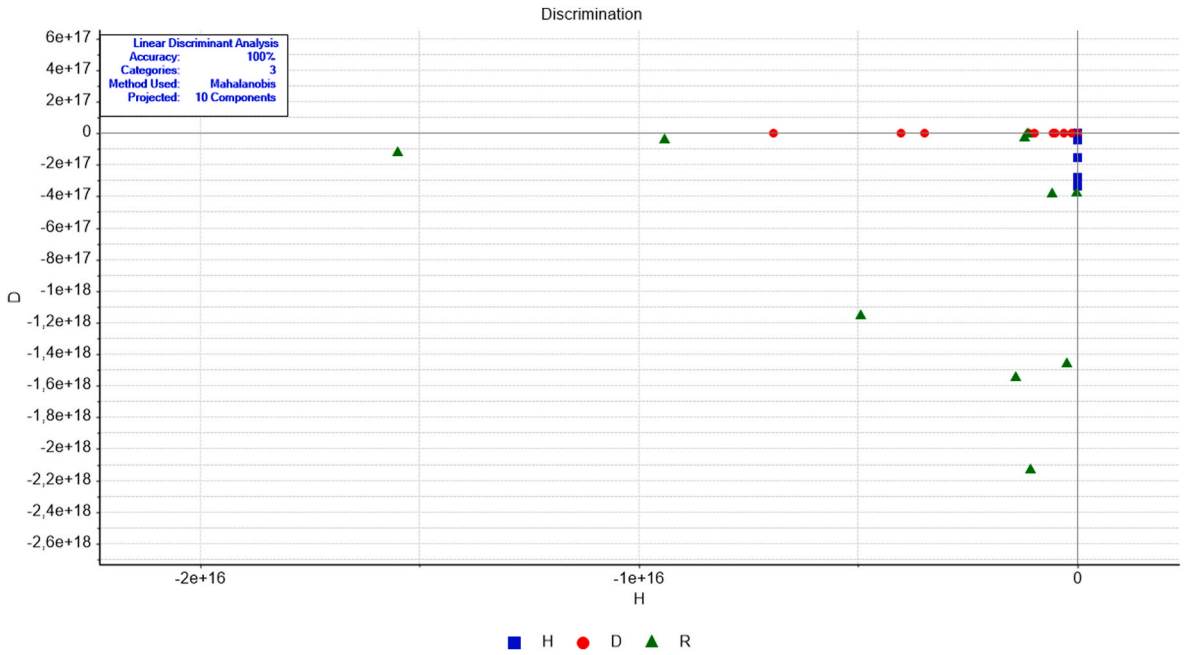

Fig. 1. The discrimination plot for newborn calf serum in a fingerprint (1800-650 cm^{-1}) infrared spectral window. The supervised Linear Discriminant Analysis (LDA) wasapplied to project 10 principal components using the Mahalanobis method. H (Healthy), D (Diseased), R (Recovered).

capability is further substantiated by the prediction and confusion matrices, which delineate the unequivocal assignment of all samples to their respective categories without misclassification (Tables 1 and 2). Table 1 presents the discriminant scores generated by LDA model for classifying serum samples from neonatal calves into three groups: H, D, and R. The values in the columns labeled H, D, R represent the Mahalanobis distances (or discriminant scores) of each sample to the centroid of each class. These scores quantify how closely a sample aligns with the spectral characteristics of the respective groups. Lower (less negative) values indicate stronger alignment with the corresponding class. For example, in the first row (an H sample), the score for the H class (−505) is significantly less negative than those for D (−147,828,800,000,000) and R (−3,784,406,000,000,000), leading the model to classify this sample as H. The predicted class for each sample (final column) is

Table 1
Prediction matrix for newborn calf serum in a fingerprint (1800-650 cm^{-1}) infrared spectral window. H (Healthy), D (Diseased), R (Recovered).

Prediction Matrix				
Actual	H	D	R	Predicted
H	−505	−147828800000000	−3784406000000000	**H**
H	−21	−1061291000000000	−27455910000000000	**H**
H	−124	−946114500000000	−13313550000000000	**H**
H	−38	−153647100000000000	−54047160000000000	**H**
H	−25	−13793710000000000	−5337004000000000	**H**
H	−28	−276594600000000000	−132017200000000000	**H**
H	−8	−336585200000000000	−26185990000000000	**H**
H	−46	−468995700000000	−4465460000000000	**H**
H	−129	−40071600000000000	−120866000000000000	**H**
H	−38	−669454500000000	−137705200000000000	**H**
D	−988981300000000	−80	−18651900000000000	**D**
D	−3476273000000000	−1406	−3280974000000000	**D**
D	−1117593000000000	−3792	−54939210000000000	**D**
D	−504517400000000	−2001	−28428820000000000	**D**
D	−4015377000000000	−945	−47114050000000000	**D**
D	−273729600000000	−12	−5398007000000000	**D**
D	−563460400000000	−2115	−22019460000000000	**D**
D	−140189400000000	−14170	−3643294000000000	**D**
D	−305365500000000	−1108	−8843089000000000	**D**
D	−6926108000000000	−6017	−33860580000000000	**D**
R	−4941371000000000	−1158686000000000000	−168	**R**
R	−1401850000000000	−1547740000000000000	−506	**R**
R	−15496940000000000	−121731900000000000	−334	**R**
R	−1066663000000000	−2136042000000000000	−53	**R**
R	−1211762000000000	−31086580000000000	−291	**R**
R	−1126716000000000	−5316285000000000	−143	**R**
R	−9413767000000000	−42447600000000000	−843	**R**
R	−244474200000000	−1459523000000000000	−48	**R**
R	−565796200000000	−385615400000000000	−62	**R**
R	−8244210000000	−377595800000000000	−1124	**R**

Table 2
Confusion matrix for newborn calf serum in a fingerprint (1800-650 cm^{-1}) infrared spectral window. H (Healthy), D (Diseased), R (Recovered).

Confusion Matrix	Actual	H	D	R
Predicted		1	2	3
H	**1**	10	0	0
D	**2**	0	10	0
R	**3**	0	0	10

determined by identifying the least negative value (i.e., the smallest Mahalanobis distance) across the H, D, and R columns. This reflects the model's confidence in assigning a sample to the class whose centroid it is closest to in the discriminant space. Furthermore, these scores reflect biochemical differences in serum spectra between groups. The perfect classification underscores the model's ability to distinguish molecular fingerprints associated with health, disease, and recovery. This result validates the LDA model's robustness and highlights its utility in non-invasive diagnosis of NCD. Additionally, the classification plot of SVM analysis revealed 100 % training and 74 % validation accuracies over the C–H stretching region (4000–2500 cm^{-1}), in which all the training set samples (27 out of 30) belonging to H, D, and R classes were correctly classified (Fig. 2). These findings underscore the robust diagnostic potential of predictive statistics, demonstrating its precision in categorizing distinct physiological states in neonatal calves through IR spectral analysis of sera.

A qualitative exploration of the complete IR spectral dataset across selected wavenumber regions revealed pronounced variations in the serum of neonatal calves (Fig. 3). Importantly, this assessment was performed on each individual spectrum rather than on the average spectra of study groups shown in Fig. 3. These average spectra were provided to facilitate visualization of the depicted changes. Two prominent alterations were visually discernible in the spectra (Fig. 3a). The first of these, observed within the C–H stretching region (4000–2500 cm^{-1}), corresponds to a distinct absorption band centered at approximately 3300 cm^{-1} (Fig. 3b). This feature is attributable to NH stretching vibrations of Amide A groups, predominantly associated with protein conformations, as established by Ref. [36]. A second notable spectral feature emerged within the fingerprint region (1800–650 cm^{-1}), characterized by a band at around 1080 cm^{-1} (Fig. 3c). This signal aligns with PO_2^- symmetric stretching modes of phosphate backbones mainly in nucleic acids and/or phospholipids, consistent with prior assignments reported by Ref. [37]. These findings highlight region-specific molecular signatures reflective of biochemical variations across physiological states in the sera of neonatal calves.

Further quantitative evaluation of the identified spectral bands demonstrated significant variations in their band areas across the neonatal calf groups (Fig. 4). The Amide A band (approximately at 3300 cm^{-1}), associated with NH stretching vibrations in proteins, exhibited a marked elevation in Diseased (D) and Recovered (R) calves relative to Healthy (H) ones. ROC analysis underscored the diagnostic utility of this band for distinguishing NCD in the D group (AUC = 0.8333); however, its discriminative power diminished in assessing recovery status (R group, AUC = 0.5926) (Fig. 4a). Conversely, the PO_2^- symmetric stretching band (near 1080 cm^{-1}), linked to nucleic acid quantities, displayed a pronounced increase in the D group, with levels reverting to baseline in the R group. This trend was corroborated by robust AUC values (D: AUC = 0.8611; R: AUC = 0.9028), affirming its sensitivity to both disease presence and recovery (Fig. 4b). To synthesize these findings, a spectrochemical index was formulated as the ratio of PO_2^- to Amide A band areas (1080 cm^{-1}/3300 cm^{-1}). Elevated index values in serum samples were indicative of active disease states, whereas reductions aligned with convalescence. ROC validation confirmed the index's diagnostic efficacy, yielding high predictive accuracy (D: AUC = 0.8750; R: AUC = 0.9219) (Fig. 4c). This index thus provides a rapid, non-invasive tool for monitoring biochemical shifts associated with disease and recovery in neonatal calves, bridging spectral data with clinical relevance.

4. Discussion

Calf diarrhea is associated with significant economic losses in the cattle industry due to mortality, growth retardation, and treatment costs. Over 50 % of pre-weaning calf mortalities are linked to diarrhea, with the majority of cases occurring in calves under one month of age

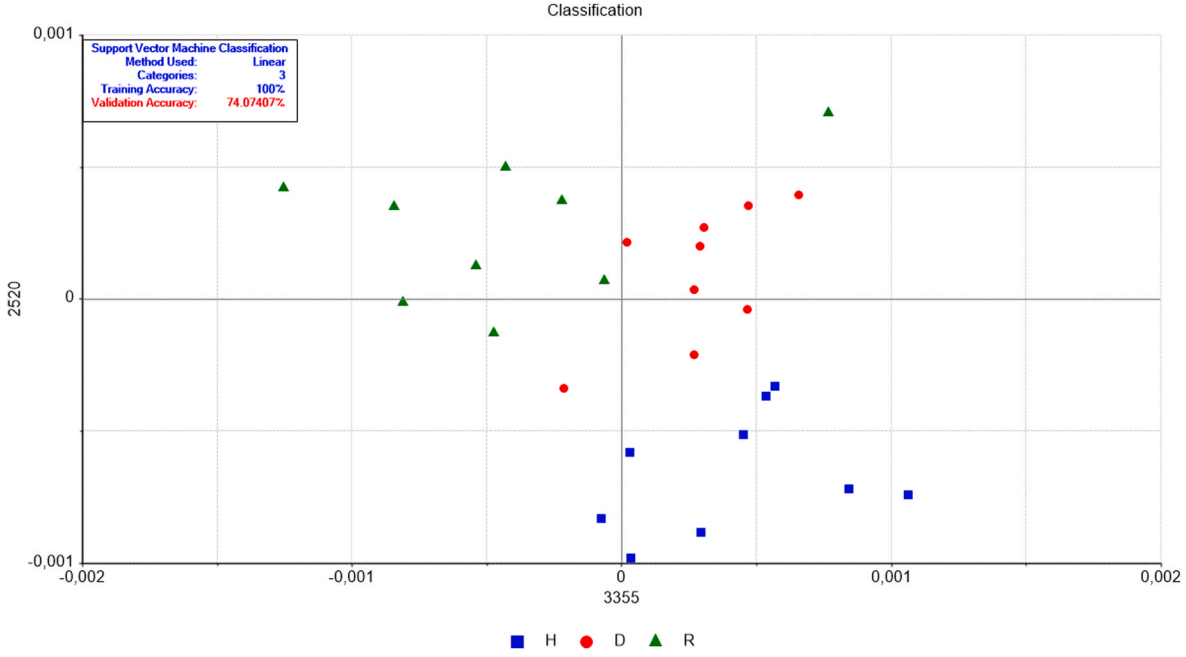

Fig. 2. The classification plot for newborn calf serum in a C–H stretching (4000-2500 cm^{-1}) infrared spectral window. The supervised Support Vector Machine (SVM) classification was applied using SVM type: Classification (nu-SVC), Kernel type: Linear, Nu value: 0.5, Weights: All 1.00, Cross-validation segments: 30. H (Healthy), D (Diseased), R (Recovered).

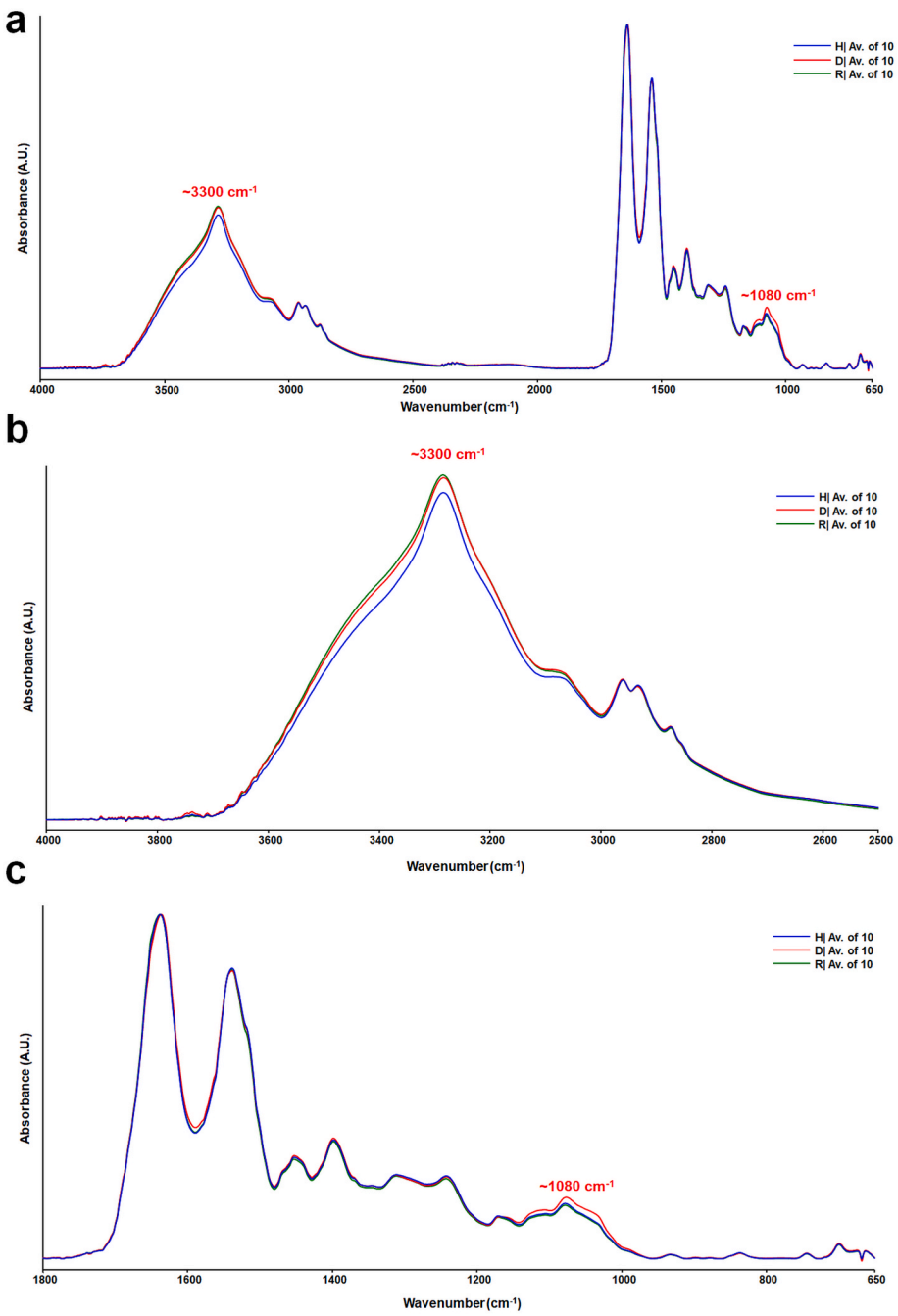

Fig. 3. The averaged, baseline-corrected, and normalized infrared spectra of newborn calf serum in **a)** full (4000-650 cm^{-1}), **b)** C–H stretching (4000-2500 cm^{-1}), and **c)** fingerprint (1800-650 cm^{-1}) windows. H (Healthy), D (Diseased), R (Recovered).

[38]. It is a significant cause of mortality and morbidity in newborn calves globally, with substantial economic repercussions. Neonatal diarrhea incidence varies globally, with the lowest rates in Sweden and Denmark (9.8–10.3 %), higher rates in Germany (37 %) and Switzerland (similar levels), and lower values in France (14.4 %) and the Netherlands (19.1 %). Diarrhea contributes to 5–10 % of newborn calf deaths and accounts for half of all mortality in calves under one month old [17,39]. In Turkey, approximately 6 million calves are born annually, and mortality attributed to diarrhea is at least 15 %, resulting in 900,000 deaths and an annual economic loss of 3.15 billion TL (525 million euros). Mortality rates vary by region and farm management: in developed European countries, rates range between 10 and 15 %, while well-managed farms report rates below 5 %. However, in poorly managed settings, mortality can escalate to 50 %, and morbidity can affect up to 100 % of calves in affected herds [40]. High mortality correlates with a 38 % reduction in farm profitability, necessitating balanced rations, colostrum management, and hygienic practices to enhance sustainability [41]. Approximately 75–80 % of diarrhea cases occur within the first week of life, with 75–95 % of gastrointestinal cases linked to infectious agents such as *Rotavirus*, *C. parvum*, and enterotoxigenic *E. coli* (ETEC) [40]. In Europe, *Rotavirus* and *Cryptosporidium* are the most prevalent pathogens. These infections are exacerbated by factors like inadequate colostrum intake, poor hygiene, and environmental stressors, leading to high morbidity and substantial long-term economic losses due to treatment costs, reduced growth rates, and diminished productivity [42]. The high prevalence of *Cryptosporidium*

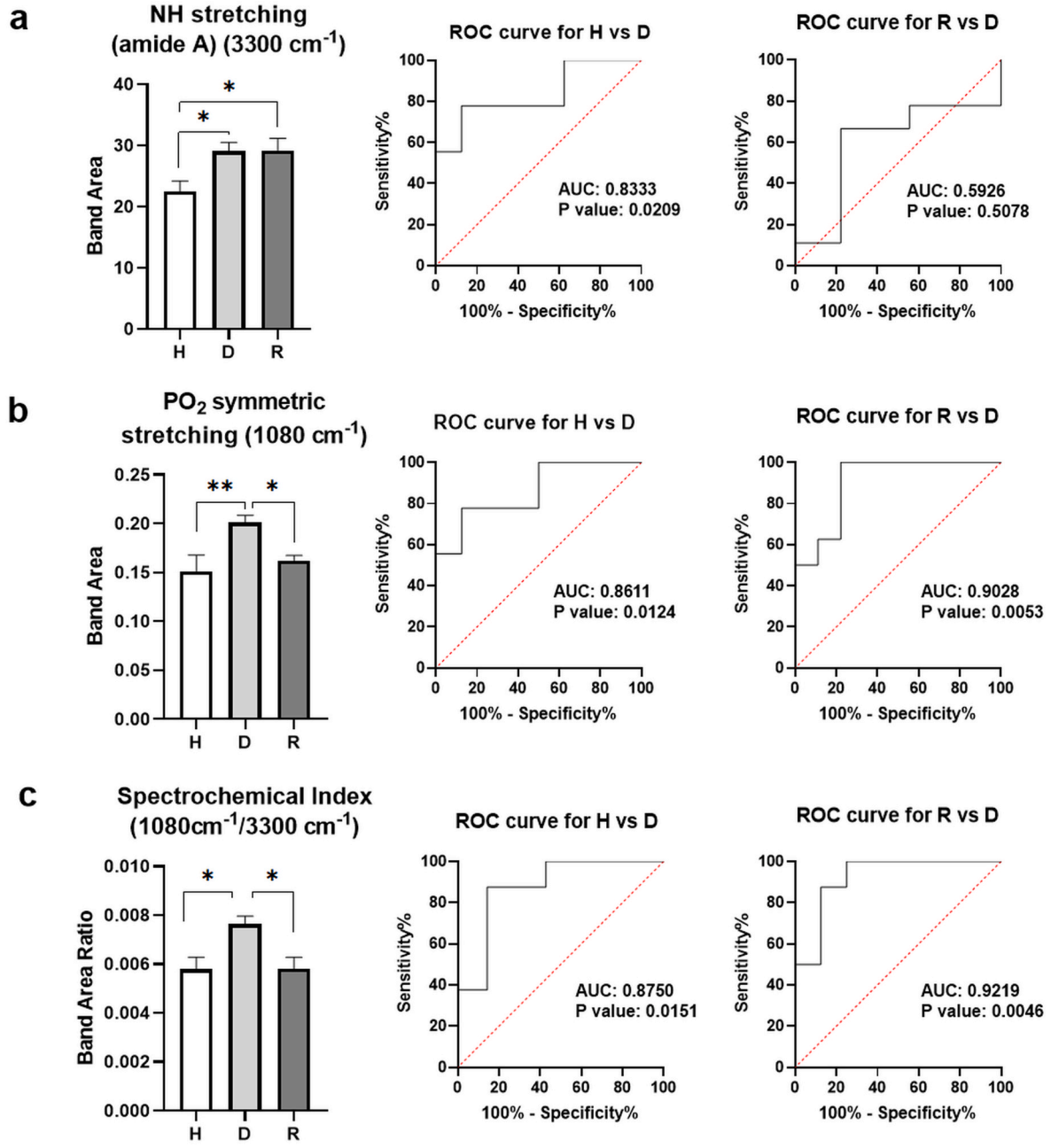

Fig. 4. The quantification of spectral bands in newborn calf serum. **a)** NH stretching Amide A band at 3300 cm^{-1}, **b)** PO_2^- symmetric stretching band at 1080 cm^{-1}, and **c)** the spectrochemical index (1080 cm^{-1}/3300 cm^{-1}). H (Healthy), D (Diseased), R (Recovered).

sp. and multidrug-resistant *E. coli* in Western Algerian diarrheic calves under 30 days old underscores regional challenges linked to hygiene, management practices, and antibiotic overuse, emphasizing the need for targeted interventions to mitigate NCD and antimicrobial resistance in Algerian livestock [43].

Diarrhea is a prevalent and economically significant disease in livestock, causing substantial losses due to reduced growth rates, increased mortality, and the costs associated with treatment and management. It is particularly severe in neonatal animals, such as calves, lambs, and piglets, whose immature immune systems render them more susceptible to infections [5]. Environmental stressors, poor hygiene, overcrowding, inadequate colostrum intake, and nutritional imbalances further predispose animals to the disease by compromising gut health and immune function [44]. For instance, failure to receive sufficient maternal antibodies through colostrum has been identified as a critical risk factor for neonatal diarrhea in ruminants [45]. Additionally, antibiotic resistance among bacterial pathogens complicates treatment, necessitating alternative strategies such as probiotics, prebiotics, and improved biosecurity measures [46]. Recent research highlights that the colostrum's bioactive components, including immunoglobulins, hormones, oligosaccharides, and microRNAs, are essential for calves' immune, intestinal, and metabolic development. At the same time, intensive milk-feeding programs optimize growth, health, and welfare by reducing hunger and supporting lifelong productivity [47]. Penazzi et al. (2025) demonstrated that oral nucleotide supplementation reduces diarrhea incidence, enhances growth, and promotes gut health in foals, likely by supporting intestinal mucosa repair and microbiota maturation. These findings suggest dietary nucleotides could be a practical intervention for improving neonatal foal health, though further research is needed to explore long-term effects and immune interactions [48].

As detailed by Foster and Smith (2009), ETEC primarily affects calves within the first days of life, utilizing K99 fimbriae to adhere to the ileal epithelium and secreting heat-stable toxin (STa) [40]. STa binds guanylyl cyclase-C, increasing intracellular cGMP, which activates chloride secretion via CFTR and inhibits sodium absorption, leading to secretory diarrhea [49,50]. *C. parvum*, prevalent in dairy calves, invades intestinal epithelial cells, inducing villous atrophy, crypt hyperplasia, and apoptosis [51]. Prostaglandins (PGE_2, PGI_2) mediate anion secretion and inhibit NaCl absorption, exacerbated by enteric nervous system (ENS) activation [52]. *Rotavirus* targets mature villous enterocytes, releasing the enterotoxin NSP4, which disrupts sodium-glucose cotransport (SGLT1), impairs disaccharidase activity via calcium signaling, and stimulates ENS-driven fluid secretion [53]. Coronavirus damages both villous and crypt enterocytes, spreading from the proximal intestine to the colon, causing prolonged malabsorption [54]. Other pathogens, such as attaching-effacing *E. coli*, *Torovirus, Clostridium difficile*, and *Giardia*, contribute variably through mechanisms like toxin production or villous damage, though their roles remain less defined. Age-dependent susceptibility, influenced by intestinal pH, receptor expression (e.g., GCC for STa), and immune maturation, further modulates disease progression. Together, these mechanisms, ranging from toxin-mediated secretion to structural gut damage, underlie the multifactorial pathogenesis of calf diarrhea [40].

Biochemical fingerprinting plays an important role in diagnosis and prognosis of infections. Previous studies employing IR spectroscopy (MIR and NIR) on virus samples highlight their utility in detecting viral infections through molecular fingerprinting [55]. Erukhimovitch et al. (2011) used MIR-FTIR with PCA to identify stage-dependent spectral changes in herpesviruses, noting increased nucleic acid signals (1220–1260 cm^{-1}) during early infection and carbohydrate bands (1023 cm^{-1}) during late stages due to host cell apoptosis [56]. Sakudo et al. (2012) applied NIR (600–1100 nm) with PCA/SIMCA to discriminate influenza-infected samples via carbohydrate/C–H group bands (850–1030 nm) [57]. Fernandes et al. (2018) leveraged NIR-PLS modeling to detect Zika infection, linking wavelengths at 1000 and 1413 nm to glycoproteins and instrumental artifacts [58]. Roy et al. (2019) utilized MIR-ATR-FTIR with second-derivative analysis to differentiate hepatitis B (HBV) and C (HCV) infections, identifying β-pleated sheet (1646 cm^{-1}) and nucleic acid (1078 cm^{-1}) markers [59]. Dou et al. (2020) employed AFM-IR to resolve MS2 bacteriophage and HSV-1 nucleic acid (808–1258 cm^{-1}) and protein (amide I/II) signatures [60]. Barauna et al. (2021) and Wood et al. (2021) applied MIR-FTIR to SARS-CoV-2, detecting viral RNA (1078–1249 cm^{-1}) and protein (1658 cm^{-1}) bands in saliva, with Barauna et al. noting host immune responses via decreased absorbance at 1220–1084 cm^{-1} [61,62]. A multivariate linear regression model (MLRM) coupled with IR spectroscopy was utilized to discriminate COVID-19 infection from human saliva samples [63]. Combined with PCA and LDA analyses, IR spectroscopy successfully discriminated bimolecular markers in *Salmonella typhi* and dengue-infected freeze-dried sera samples along with healthy freeze-dried sera samples [64]. A recent study revealed that Amide A and PO_2^- symmetric stretching spectral bands, in combination with PCA and LDA tools, can distinguish metastatic lymph nodes from non-metastatic ones [65]. These biochemical marker bands and complementary PCA, ROC, and SVM tools were also helpful for the diagnosis and monitoring of polycythemia vera disease from sera [66]. Combined with complementary biomarkers and ML-based analytical methods, these biomarkers enable rapid, non-invasive diagnosis and reflect underlying molecular mechanisms, advancing clinical translation of IR spectroscopy for autoimmune and neurodegenerative diseases [37]. Collectively, these studies underscore MIR's dominance for direct molecular analysis (e.g., nucleic acids, proteins) and NIR's reliance on computational methods (PCA/PLS) to resolve overlapping spectral features. Recent efforts emphasize MIR's role in rapid, non-invasive SARS-CoV-2 diagnostics, demonstrating the potential of IR spectroscopy for label-free virus detection and host response monitoring.

The 3300 cm^{-1} (Amide A) and 1080 cm^{-1} (PO_2^- symmetric stretching) bands, together with several other spectral bands, were proposed as potential biochemical markers for the characterization of human cerebral tissues [67], human substantia nigra in Parkinson's disease [68], and for diagnosis of bladder cancer malignancies [69]. Alterations in these bands can serve as biomarkers for pathological conditions such as protein aggregation in neurodegeneration or DNA damage in cancer [70]. These spectral bands are indispensable tools for understanding biomolecular structure-function relationships, offering insights into health, disease, and therapeutic development [71,72]. The Amide A band serves as a valuable, though underutilized, tool for probing hydrogen bonding environments and protein dynamics [73]. Its applications in structural biology, diagnostics, and biophysics are promising, particularly with advancements in spectroscopic techniques addressing its inherent challenges. Monitoring Amide A helps assess structural changes in amyloid protein-associated protein dynamics, which is critical in diseases associated with amyloid dysregulation, where misfolding occurs [74]. The 3300 cm^{-1} spectral band corresponds to Amide A bands stemming from NH stretching vibrations of proteins and nucleic acids and has emerged as a critical marker in disease diagnostics and mechanistic studies [36,75–79]. The band is also one of the characteristic serum spectral bands utilized for rapidly diagnosing various rheumatic immune diseases [80,81]. Amide A also exhibits notable changes in the cardiac tissues of victims who died because of Old Myocardial Infarction (OMI), highlighting its potential as a biomarker for diagnosing atypical OMI presentations [82]. Furthermore, inflammatory diseases exhibit altered spectral profiles in this region. It is well-documented that the spectral band around 1080 cm^{-1} emerges from the PO_2^- symmetric stretching of nucleic acids and/or phospholipids [83]. Its frequency and shape depend on interactions with cations such as $Mg^{2+}$and Na^+, hydration, and backbone conformation [70,84]. In phospholipids, PO_2 vibrations report on lipid bilayer organization and interactions with proteins or ions, relevant to membrane fluidity and signaling [66]. Investigations into COVID-19 infections have revealed elevated nucleic acid levels in disease-positive biofluids, including serum and saliva [28,62,63,85]. This phenomenon may be linked to systemic inflammation triggered by severe infections, which correlate with heightened cell-free DNA (cfDNA) concentrations in circulation. These findings underscore the utility of the 3300 cm-^{1} and 1080 cm^{-1} bands as a non-invasive, label-free spectral biomarker for probing molecular-level metabolic alterations in disease mechanisms and advancing early diagnostic strategies.

The 1080 cm^{-1}/3300 cm^{-1} index is a quantitative and valid spectral biomarker derived in this study by calculating the ratio of the integrated band areas at 1080 cm^{-1} and 3300 cm^{-1}. As mentioned above, the 1080 cm^{-1} band is primarily associated with PO_2^- symmetric stretching, which reflects the concentration of nucleic acids and phospholipids in the serum, while the 3300 cm^{-1} band corresponds to Amide A vibrations, indicative of protein NH stretching and, thus, protein structure and content. The alteration of Amide A band likely reflects inflammation-driven changes in the protein milieu. During a systemic inflammatory response, proinflammatory cytokines (TNF-α, IL-1β) and stress hormones induce a pronounced catabolic state that accelerates protein turnover and breakdown [86]. In NCD, severe infection triggers an acute-phase response with elevated plasma proteins (for example, haptoglobin increases markedly in calves with serious diarrhea [87]) alongside extensive tissue protein catabolism. This de novo surge of acute-phase proteins and concurrent proteolysis can broaden or intensify the amide spectral bands by increasing circulating peptides and altering protein conformation. In essence, the heightened Amide A signal in sick calves is consistent with inflammation-induced protein changes – a combination of cytokine-driven acute phase protein production and protein degradation due to the body's "autocatabolic" response to infection [86]. Such inflammation-mediated protein dynamics, including immunoglobulin fluctuations and muscle protein loss can provide a biological basis for the observed 3300 cm^{-1} IR alterations

in diarrheic neonates, beyond general biochemical variation.

An increase at 1080 cm^{-1} signals a higher concentration of nucleic acid components – most plausibly cell-free DNA (cfDNA) and RNA fragments circulating in the bloodstream. In the context of NCD's immune response, a rise in cfDNA is indicative of extensive cell death and immune cell turnover. Severe systemic inflammation is known to cause widespread cellular injury; high levels of circulating cfDNA are a well-established hallmark of tissue damage and SIRS (systemic inflammatory response syndrome) [88,89]. Mechanistically, proinflammatory cytokine cascades and pathogen toxins trigger apoptosis in both immune cells and peripheral tissues, while activated neutrophils may undergo NETosis (releasing neutrophil extracellular traps composed of DNA). These processes flood the extracellular space with nucleic acids, which the IR spectrum captures as an amplified PO_2^- band [89]. Notably, the cfDNA released during inflammation does not merely mark cellular demise, it can further propagate immune activation by acting as a DAMP (damage-associated molecular pattern). Often bound to histones, extracellular DNA stimulates pattern recognition receptors (TLR9, STING pathway), thereby amplifying inflammation, cytokine release, and even coagulation [90]. This positive-feedback loop links the heightened 1080 cm^{-1} signal directly to ongoing immunopathological events. In summary, the spectral elevation at ~1080 cm^{-1} in diarrheic neonates reflects the immunological "footprint" of NCD: an abundance of nucleic acid debris from dying cells and neutrophil traps, in line with vigorous inflammation and immune cell turnover. In the context of NCD, an elevated 1080 cm^{-1}/3300 cm^{-1} index suggests an increased presence of nucleic acids and phospholipids, which may arise from inflammatory responses, cellular turnover, or tissue damage associated with the disease. Conversely, a lower index is indicative of a return toward normal biochemical conditions as the calf recovers. By monitoring these spectral changes, the index provides a rapid, non-invasive tool for assessing the disease state and tracking recovery, effectively bridging molecular-level information with clinical diagnosis.

Predictive analytics and ML techniques have emerging applications in veterinary contexts, particularly for diagnosing and managing various livestock diseases. A recent review by Prosser et al. (2025) highlighted that ML and artificial intelligence (AI) offer transformative potential in BRD diagnostics and management through applications such as pathogen identification via metagenomic sequencing, predictive epidemiological models, and sensor-based technologies for early symptom detection. Key advancements include computer-aided lung auscultation (CALA) devices and wearable sensors achieving high accuracy (up to 98.8 %) in fever detection, though many models still require refinement for commercial use. Despite challenges like data management and variable performance, integrating ML/AI with traditional methods enhances diagnostic objectivity, efficiency, and decision-making, promising cost-effective and labor-saving strategies for BRD control in cattle industries [91]. It was reported that the convolutional neural network (CNN) model achieved 73.89 % accuracy in detecting lumpy skin disease (LSD) in calves using image data, highlighting the potential of AI for early disease diagnosis in veterinary medicine. Integrating diverse data sources and leveraging complex models like CNNs can enhance prediction accuracy, even with limited data, offering a pathway to improve animal welfare and sustainable livestock farming through proactive disease management [92]. Taneja et al. (2020) developed a fog computing and ML system for early lameness detection in dairy cattle using pedometers to monitor activity data. The hybrid clustering-classification model achieved 87 % accuracy in detecting lameness three days before visual signs appeared, while fog processing reduced cloud data transfer by 84 %. Validated on 150 cows, the approach offers scalable, cost-effective monitoring and timely intervention to improve animal welfare and farm productivity [93]. It was highlighted that ML algorithms such as Random Forest, SVM, and deep learning models (CNNs, LSTMs) effectively enable the early detection of cattle diseases, achieving high accuracy (up to 95.9 %) by integrating diverse data sources like IoT sensors, wearable devices, and environmental factors. These technologies enhance livestock health management by enabling proactive disease prevention, improving diagnostic precision, and supporting informed decision-making for farmers [94]. IR thermography (IRT) and ML enabled non-invasive, automated cattle health monitoring by detecting diseases (mastitis, lameness), physiological traits, stress, and oestrus through thermal imaging and advanced analytics [95]. The study by Senthilkumar et al. (2024) evaluated ten pretrained deep learning models for early detection of LSD in cattle, with VGG16 and MobileNetV2 emerging as the most effective, achieving accuracies of 96.07 % and 96.39 %, respectively. These models demonstrated high sensitivity and specificity, proving their potential as AI-driven tools for reliable LSD diagnosis, ultimately benefiting livestock health and agricultural economies [96]. It was demonstrated that LAP-MALDI MS, combined with ML, enables rapid, cost-effective, and high-throughput disease diagnostics. It successfully detected bovine mastitis up to two days before clinical symptoms appeared with 70 % sensitivity and 100 % specificity while also proving effective in identifying antimicrobial resistance through lactamase activity analysis [97].

The predictive classification platform developed in this study ingeniously combines IR spectroscopy with ML algorithms to diagnose neonatal diarrhea in calves rapidly, non-invasively, and accurately. By capturing the unique spectral fingerprints of serum samples, the system employs PCA to distill key spectral features and then applies LDA and SVM for robust classification of healthy, diseased, and recovered calves. This seamless integration of rapid, non-invasive spectral analysis with predictive analytics not only enhances diagnostic precision and timeliness but also offers a scalable, cost-effective tool that supports proactive disease management and sustainable livestock practices. While the developed platform achieved clear spectral discrimination among healthy, diseased, and recovered calves, it is important to note that this proof-of-concept study was conducted on a relatively small cohort, that are 30 serum samples (10 per group). A limited number of independent biological replicates can inflate apparent classification accuracy and may not fully capture inter-animal variability. To enhance model robustness and ensure broad applicability, future work should involve substantially larger and more diverse sample sets, ideally collected from multiple farms and geographic regions. Increasing the sample size would allow for better estimation of true sensitivity and specificity, and the exploration of potential confounders or sub-phenotypes. Such efforts will be critical to translating this spectral-machine-learning framework into a universally reliable, on-farm diagnostic tool for NCD.

To further clarify the selection of model parameters, it is important to elaborate on the role of the higher-order PCs used in the PCA-LDA framework. The retention of 10 PCs was not arbitrary but based on both explained variance profiles and the interpretability of the component loadings. While the first few PCs (PC1–PC3) accounted for the majority of variance, they primarily captured global spectral trends related to overall sample differences. The higher-order PCs (PC4–PC10), though contributing progressively smaller portions of variance, encoded subtle, localized spectral variations that were essential for enhancing class discrimination. Importantly, these components exhibited structured and interpretable loading patterns across key spectral regions rather than random noise, confirming that they captured biologically meaningful signals rather than overfitting artifacts.

Incorporating these higher-order PCs was critical for improving classification robustness, as evidenced by the LDA discriminant function coefficients drawing on multiple PCs across the full retained set. This indicates that class-separating information is distributed across both dominant and more nuanced spectral features. Moreover, cumulative explained variance analysis demonstrated that retaining 10 PCs struck a balance between model complexity and generalizability, avoiding underfitting while minimizing overfitting risk. These findings are consistent with the notion that clinically relevant biochemical changes associated with disease and recovery are reflected not only in major spectral trends but also in subtle spectral shifts, which higher-order PCs

effectively capture.

5. Conclusion

In conclusion, this proof-of-concept study presents a robust and innovative diagnostic platform that integrates ATR-FTIR spectroscopy with advanced predictive analytics to rapidly and non-invasively diagnose NCD. By capturing unique serum biochemical fingerprints and leveraging both LDA and SVM algorithms, the system achieved high classification accuracy in distinguishing healthy, diseased, and recovered calves. Notably, the integration of complex spectral data into a single, interpretable parameter, exemplified by the 1080 cm^{-1}/3300 cm^{-1} spectrochemical index, further enhanced diagnostic precision by correlating molecular-level changes with clinical status, providing a clear and valid biomarker of disease progression and recovery. This scalable, cost-effective approach facilitates timely therapeutic interventions and improves on-farm decision-making and holds significant promises for advancing sustainable livestock management and reducing the economic impact of NCD.

CRediT authorship contribution statement

Nuri Ceran: Software, Methodology, Formal analysis. **Rafig Gurbanov:** Writing – review & editing, Writing – original draft, Visualization, Validation, Supervision, Software, Resources, Project administration, Methodology, Investigation, Formal analysis, Data curation, Conceptualization.

Consent to participate

Consent to participate is not required in this study.

Ethics approval

This study was carried out with the approval of the Local Animal Experiments Ethics Committee of Niğde Ömer Halis Demir University (Approval No: E−86837521-050.99-257260).

Consent for publication

Consent for publication is not required in this study.

Availability of data and material

All data generated during and/or analyzed during the current study are available from the corresponding author upon reasonable request.

AI declaration

No generative AI or AI-assisted technologies were used in the generation of the research data, analysis, or conclusions presented in this manuscript. All data collection, processing, and interpretation were conducted using conventional analytical and statistical methods, including ATR-FTIR spectroscopy and machine learning algorithms implemented through standard software tools. Any AI-based predictive analytics applied in this study, such as machine learning classification models, were explicitly used for data analysis and not for content generation. The manuscript was written entirely by the authors without the use of AI-assisted text-generation tools except for paraphrasing and grammar checking.

Funding

This research was partially funded by the TUBİTAK BİDEB-2209A program (Project no: 1919B012109444).

Declaration of competing interest

The authors declare that they have no known competing financial interests or personal relationships that could have appeared to influence the work reported in this paper.

Acknowledgments

The authors are grateful to the Department of Chemistry at Bilecik Şeyh Edebali University for providing an FTIR spectrometer.

Data availability

Data will be made available on request.

References

[1] D.J. Wilson, G. Habing, C.B. Winder, D.L. Renaud, A scoping review of neonatal calf diarrhea case definitions. https://www.elsevier.com/open-access/userlicense/1.0/, 2022.
[2] Y. Muktar, G. Mamo, B. Tesfaye, D. Belina, A review on major bacterial causes of calf diarrhea and its diagnostic method, J. Veterinary Med. Animal Health 7 (2015) 173–185, https://doi.org/10.5897/JVMAH2014.
[3] D.R. Smith, Field disease diagnostic investigation of neonatal calf diarrhea, Vet. Clin. Food Anim. Pract. 28 (2012) 465–481, https://doi.org/10.1016/j.cvfa.2012.07.010.
[4] M.M. Izzo, P.D. Kirkland, V.L. Mohler, N.R. Perkins, A.A. Gunn, J.K. House, Prevalence of major enteric pathogens in Australian dairy calves with diarrhoea, Aust. Vet. J. 89 (2011), https://doi.org/10.1111/j.1751-0813.2011.00692.x.
[5] Y. il Cho, K.J. Yoon, An overview of calf diarrhea - infectious etiology, diagnosis, and intervention, J. Vet. Sci. 15 (2014) 1–17, https://doi.org/10.4142/jvs.2014.15.1.1.
[6] M.C. Windeyer, K.E. Leslie, S.M. Godden, D.C. Hodgins, K.D. Lissemore, S. J. LeBlanc, Factors associated with morbidity, mortality, and growth of dairy heifer calves up to 3 months of age, Prev. Vet. Med. 113 (2014), https://doi.org/10.1016/j.prevetmed.2013.10.019.
[7] N.J. Urie, J.E. Lombard, C.B. Shivley, C.A. Kopral, A.E. Adams, T.J. Earleywine, J. D. Olson, F.B. Garry, Preweaned heifer management on US dairy operations: Part V. Factors associated with morbidity and mortality in preweaned dairy heifer calves, J. Dairy Sci. 101 (2018), https://doi.org/10.3168/jds.2017-14019.
[8] E. Jessop, L. Li, D.L. Renaud, A. Verbrugghe, J. Macnicol, L. Gamsjäger, D. E. Gomez, Neonatal calf diarrhea and gastrointestinal microbiota: etiologic agents and microbiota manipulation for treatment and prevention of diarrhea, Vet. Sci. 11 (2024), https://doi.org/10.3390/vetsci11030108.
[9] E.T. Kim, S.J. Lee, T.Y. Kim, H.G. Lee, R.M. Atikur, B.H. Gu, D.H. Kim, B.Y. Park, J. K. Son, M. Kim, Dynamic changes in fecal microbial communities of neonatal dairy calves by aging and diarrhea, Animals 11 (2021), https://doi.org/10.3390/ani11041113.
[10] D.E. Gomez, L.G. Arroyo, M.C. Costa, L. Viel, J.S. Weese, Characterization of the fecal bacterial microbiota of healthy and diarrheic dairy calves, J. Vet. Intern. Med. 31 (2017), https://doi.org/10.1111/jvim.14695.
[11] C.J.M. Bartels, M. Holzhauer, R. Jorritsma, W.A.J.M. Swart, T.J.G.M. Lam, Prevalence, prediction and risk factors of enteropathogens in normal and non-normal faeces of young Dutch dairy calves, Prev. Vet. Med. 93 (2010), https://doi.org/10.1016/j.prevetmed.2009.09.020.
[12] I. Lorenz, R. Huber, F.M. Trefz, A high plane of nutrition is associated with a lower risk for neonatal calf diarrhea on bavarian dairy farms, Animals 11 (2021), https://doi.org/10.3390/ani11113251.
[13] H.S.M. Carter, D.L. Renaud, M.A. Steele, A.J. Fischer-Tlustos, J.H.C. Costa, A narrative review on the unexplored potential of colostrum as a preventative treatment and therapy for diarrhea in neonatal dairy calves, Animals 11 (2021), https://doi.org/10.3390/ani11082221.
[14] P.D. Constable, F.M. Trefz, I. Sen, J. Berchtold, M. Nouri, G. Smith, W. Grünberg, Intravenous and oral fluid therapy in neonatal calves with diarrhea or sepsis and in adult cattle, Front. Vet. Sci. 7 (2021), https://doi.org/10.3389/fvets.2020.603358.
[15] J. Berchtold, Treatment of calf diarrhea: intravenous fluid therapy. Veterinary Clinics of North America - Food Animal Practice 25, 2009, https://doi.org/10.1016/j.cvfa.2008.10.001.
[16] M. Kaduková, A. Schreiberová, P. Mudroň, C. Tóthová, P. Gomulec, G. Štrkolcová, Cryptosporidium infections in neonatal calves on a dairy farm, Microorganisms 12 (2024), https://doi.org/10.3390/microorganisms12071416.
[17] K. Schwaiger, J. Storch, C. Bauer, J. Bauer, Lactobacillus (Limosilactobacillus) reuteri: a probiotic candidate to reduce neonatal diarrhea in calves, Front. Microbiol. 14 (2023), https://doi.org/10.3389/fmicb.2023.1266905.
[18] S.S. Nielsen, J. Alvarez, D.J. Bicout, P. Calistri, E. Canali, J.A. Drewe, B. Garin-Bastuji, J.L. Gonzales Rojas, C. Gortazar Schmidt, M. Herskin, V. Michel, M. A. Miranda Chueca, B. Padalino, P. Pasquali, H.C. Roberts, H. Spoolder, K. Stahl, A. Velarde, A. Viltrop, M.B. Jensen, S. Waiblinger, D. Candiani, E. Lima, O. Mosbach-Schulz, Y. Van der Stede, M. Vitali, C. Winckler, Welfare of calves, EFSA J. 21 (2023), https://doi.org/10.2903/j.efsa.2023.7896.

[19] Y.S. Malik, A.K. Verma, N. Kumar, N. Touil, K. Karthik, R. Tiwari, D.P. Bora, K. Dhama, S. Ghosh, M.G. Hemida, A.S. Abdel-Moneim, K. Bányai, A.N. Vlasova, N. Kobayashi, R.K. Singh, Advances in diagnostic approaches for viral etiologies of diarrhea: from the lab to the field, Front. Microbiol. 10 (2019), https://doi.org/10.3389/fmicb.2019.01957.
[20] M.E. Schroeder, M.A. Bounpheng, S. Rodgers, R.J. Baker, W. Black, H. Naikare, B. Velayudhan, L. Sneed, B. Szonyi, A. Clavijo, Development and performance evaluation of calf diarrhea pathogen nucleic acid purification and detection workflow, J. Vet. Diagn. Invest. 24 (2012), https://doi.org/10.1177/1040638712456976.
[21] O. Ates, K. Yesilbag, Characterization of bovine rotavirus isolates from diarrheic calves in Türkiye, Mol. Biol. Rep. 50 (2023) 3063–3071, https://doi.org/10.1007/s11033-022-08169-4.
[22] O. Özturkler, S. Kızıltepe, H. Alkan, S. Hacıömeroglu, O. Ozturkler, Investigation of some microbial and protozoon factors with rapid test kits in neonatal diarrheas in calves in Kars province, J. One Health Res. 1 (2023) 1–6, https://doi.org/10.5281/zenodo.7513438.
[23] M. Santos-Rivera, A. Woolums, M. Thoresen, E. Blair, V. Jefferson, F. Meyer, C. K. Vance, Profiling Mannheimia haemolytica infection in dairy calves using near infrared spectroscopy (NIRS) and multivariate analysis (MVA), Sci. Rep. 11 (2021), https://doi.org/10.1038/s41598-021-81032-x.
[24] I. Elsohaby, J.T. McClure, C.B. Riley, R.A. Shaw, G.P. Keefe, Quantification of bovine immunoglobulin G using transmission and attenuated total reflectance infrared spectroscopy, J. Vet. Diagn. Invest. 28 (2016) 30–37, https://doi.org/10.1177/1040638715613101.
[25] Y.G. Marangoni-Ghoreyshi, T. Franca, J. Esteves, A. Maranni, K.D. Pereira Portes, C. Cena, C.R.B. Leal, Multi-resistant diarrheagenic Escherichia coli identified by FTIR and machine learning: a feasible strategy to improve the group classification, RSC Adv. 13 (2023) 24909–24917, https://doi.org/10.1039/d3ra03518b.
[26] B.A. Baspinar N, NMR based metabolomics evaluation in neonatal calves with acute diarrhea and suspected sepsis: a new approach for Biomarker/S, J. Postgenomics Drug Biomarker Develop. 4 (2014), https://doi.org/10.4172/2153-0769.1000134.
[27] A. Dogan, R. Gurbanov, M. Severcan, F. Severcan, CoronaVac (Sinovac) COVID-19 vaccine-induced molecular changes in healthy human serum by infrared spectroscopy coupled with chemometrics, Turk. J. Biol. 45 (2021) 549–558, https://doi.org/10.3906/biy-2105-65.
[28] G. Tokgoz, K.K. Kirboga, F. Ozel, S. Yucepur, I. Ardahanli, R. Gurbanov, Spectrochemical and explainable artificial intelligence approaches for molecular level identification of the status of critically ill patients with COVID-19, Talanta 279 (2024) 126652, https://doi.org/10.1016/J.TALANTA.2024.126652.
[29] Ö.K. İzgördü, R. Gurbanov, C. Darcan, Understanding the transition to viable but non-culturable state in Escherichia coli W3110: a comprehensive analysis of potential spectrochemical biomarkers, World J. Microbiol. Biotechnol. 40 (2024) 203, https://doi.org/10.1007/s11274-024-04019-6.
[30] R. Gurbanov, H. Karadağ, S. Karaçam, G. Samgane, Tapioca starch modulates cellular events in oral probiotic Streptococcus salivarius strains, Probiotics Antimicrob Proteins 13 (2021) 195–207, https://doi.org/10.1007/s12602-020-09678-z.
[31] CAMO Software AS, The unscrambler X. Help/contents, 2019.
[32] T. Ceylani, H.T. Teker, S. Keskin, G. Samgane, E. Acikgoz, R. Gurbanov, The rejuvenating influence of young plasma on aged intestine, J. Cell Mol. Med. 27 (2023) 2804–2816, https://doi.org/10.1111/jcmm.17926.
[33] İ. Ardahanlı, H.İ. Özkan, F. Özel, R. Gurbanov, H.T. Teker, T. Ceylani, Infrared spectrochemical findings on intermittent fasting-associated gross molecular modifications in rat myocardium, Biophys. Chem. 289 (2022) 106873, https://doi.org/10.1016/J.BPC.2022.106873.
[34] H.T. Teker, T. Ceylani, S. Keskin, G. Samgane, S. Mansuroglu, B. Baba, H. Allahverdi, E. Acıkgoz, R. Gurbanov, Age-related differences in response to plasma exchange in male rat liver tissues: insights from histopathological and machine-learning assisted spectrochemical analyses, Biogerontology 24 (2023), https://doi.org/10.1007/s10522-023-10032-3.
[35] A.I. Belousov, S.A. Verzakov, J. Von Frese, Applicational aspects of support vector machines, J. Chemom. (2002), https://doi.org/10.1002/cem.744.
[36] A.C.S. Talari, M.A.G. Martinez, Z. Movasaghi, S. Rehman, I.U. Rehman, Advances in Fourier transform infrared (FTIR) spectroscopy of biological tissues, Appl. Spectrosc. Rev. 52 (2017), https://doi.org/10.1080/05704928.2016.1230863.
[37] F. Severcan, I. Ozyurt, A. Dogan, M. Severcan, R. Gurbanov, F. Kucukcankurt, B. Elibol, I. Tiftikcioglu, E. Gursoy, M.N. Yangin, Y. Zorlu, Decoding myasthenia gravis: advanced diagnosis with infrared spectroscopy and machine learning, Sci. Rep. 14 (2024) 19316, https://doi.org/10.1038/s41598-024-66501-3.
[38] S.H. Lee, H.Y. Kim, E.W. Choi, D. Kim, Causative agents and epidemiology of diarrhea in Korean native calves, J. Vet. Sci. 20 (2019), https://doi.org/10.4142/jvs.2019.20.e64.
[39] K. Schwaiger, J. Storch, C. Bauer, J. Bauer, Abundance of selected bacterial groups in healthy calves and calves developing diarrhea during the first week of life: are there differences before the manifestation of clinical symptoms? Front. Microbiol. 13 (2022) https://doi.org/10.3389/fmicb.2022.958080.
[40] D.M. Foster, G.W. Smith, Pathophysiology of diarrhea in calves, Vet. Clin. Food Anim. Pract. 25 (2009), https://doi.org/10.1016/j.cvfa.2008.10.013.
[41] M.A. Karslı, Ş. Evci, The importance of cattle and calf nutrition in preventing calf losses, Lalahan Hayvan Araştırma Enstitüsü, Dergisi 58 (2018) pages 23–34.
[42] M. Şahal, O.S. Terzi, E. Ceylan, E. Kara, Calf diarrhea and prevention methods, Prev. Vet. Med. 58 (2018).
[43] S.M.A. Selles, M. Kouidri, B.T. Belhamiti, A.A. Amrane, A.R. Benia, S. M. Hammoudi, R. Kaidi, L. Boukraa, Enteropathogens associated with neonatal calves diarrhea in Tiaret area (Western Algeria), Veterinaria 67 (2018).
[44] I. Lorenz, J. Fagan, S.J. More, Calf health from birth to weaning. II. Management of diarrhoea in pre-weaned calves, Ir. Vet. J. 64 (2011), https://doi.org/10.1186/2046-0481-64-9.
[45] S.M. Godden, J.E. Lombard, A.R. Woolums, Colostrum management for dairy calves, in: Veterinary Clinics of North America - Food Animal Practice, vol. 35, 2019, https://doi.org/10.1016/j.cvfa.2019.07.005.
[46] T.R. Callaway, T.S. Edrington, R.C. Anderson, R.B. Harvey, K.J. Genovese, C. N. Kennedy, D.W. Venn, D.J. Nisbet, Probiotics, prebiotics and competitive exclusion for prophylaxis against bacterial disease, Anim. Health Res. Rev. Conference Res. Worker Animal Diseases 9 (2008), https://doi.org/10.1017/S1466252308001540.
[47] I. Lorenz, Calf health from birth to weaning - an update, Ir. Vet. J. 74 (2021), https://doi.org/10.1186/s13620-021-00185-3.
[48] L. Penazzi, E. Pagliara, T. Nervo, U. Ala, A. Bertuglia, G. Romano, J. Hattab, P. G. Tiscar, S. Bergagna, G. Pagliasso, S. Antoniazzi, L. Cavallarin, E. Valle, L. Prola, Dietary supplementation of new-born foals with free nucleotides positively affects neonatal diarrhoea management, Ir. Vet. J. 78 (2025) 7, https://doi.org/10.1186/s13620-025-00294-3.
[49] R.A. Argenzio, Pathophysiology of Neonatal Calf Diarrhea, Veterinary Clin .North America: Food Animal Prac. 1 (1985) 461–469, https://doi.org/10.1016/S0749-0720(15)31296-2.
[50] M. Field, C.E. Semrad, Toxigenic diarrheas, congenital diarrheas, and cystic fibrosis: Disorders of intestinal ion transport, Annu. Rev. Physiol. 55 (1993), https://doi.org/10.1146/annurev.ph.55.030193.003215.
[51] D.M. Ojcius, J.L. Perfettini, A. Bonnin, F. Laurent, Caspase-dependent apoptosis during infection with Cryptosporidium parvum, Microb. Infect. 1 (1999), https://doi.org/10.1016/S1286-4579(99)00246-4.
[52] R.A. Argenzio, J. Lecce, D.W. Powell, Prostanoids inhibit intestinal NaCl absorption in experimental porcine cryptosporidiosis, Gastroenterology 104 (1993), https://doi.org/10.1016/0016-5085(93)90412-6.
[53] A.P. Morris, J.K. Scott, J.M. Ball, C.Q.Y. Zeng, W.K. O'Neal, M.K. Estes, NSP4 elicits age-dependent diarrhea and Ca2+-mediated I- influx into intestinal crypts of CF mice, Am. J. Physiol. Gastrointest. Liver Physiol. 277 (1999), https://doi.org/10.1152/ajpgi.1999.277.2.g431.
[54] L.D. Lewis, R.W. Phillips, Pathophysiologic changes due to coronavirus-induced diarrhea in the calf, J. Am. Vet. Med. Assoc. 173 (1978).
[55] M.I. Rumaling, F.P. Chee, A. Bade, N.H. Hasbi, S. Daim, F. Juhim, M. Duinong, R. Rasmidi, Methods of optical spectroscopy in detection of virus in infected samples: a review, Heliyon 8 (2022) e10472, https://doi.org/10.1016/j.heliyon.2022.e10472.
[56] V. Erukhimovitch, E. Bogomolny, M. Huleihil, M. Huleihel, Infrared spectral changes identified during different stages of herpes viruses infection in vitro, Analyst 136 (2011), https://doi.org/10.1039/c1an15319f.
[57] A. Sakudo, K. Baba, K. Ikuta, Discrimination of influenza virus-infected nasal fluids by Vis-NIR spectroscopy, Clin. Chim. Acta 414 (2012), https://doi.org/10.1016/j.cca.2012.08.022.
[58] J.N. Fernandes, L.M.B. Dos Santos, T. Chouin-Carneiro, M.G. Pavan, G.A. Garcia, M.R. David, J.C. Beier, F.E. Dowell, R. Maciel-de-Freitas, M.T. Sikulu-Lord, Rapid, noninvasive detection of Zika virus in Aedes aegypti mosquitoes by near-infrared spectroscopy, Sci. Adv. 4 (2018), https://doi.org/10.1126/sciadv.aat0496.
[59] S. Roy, D. Perez-Guaita, S. Bowden, P. Heraud, B.R. Wood, Spectroscopy goes viral: diagnosis of hepatitis B and C virus infection from human sera using ATR-FTIR spectroscopy, Clin. Spectrosc. 1 (2019), https://doi.org/10.1016/j.clispe.2020.100001.
[60] T. Dou, Z. Li, J. Zhang, A. Evilevitch, D. Kurouski, Nanoscale structural characterization of individual viral particles using atomic force microscopy infrared spectroscopy (AFM-IR) and tip-enhanced Raman spectroscopy (TERS), Anal. Chem. 92 (2020), https://doi.org/10.1021/acs.analchem.0c01971.
[61] V.G. Barauna, M.N. Singh, L.L. Barbosa, W.D. Marcarini, P.F. Vassallo, J.G. Mill, R. Ribeiro-Rodrigues, L.C.G. Campos, P.H. Warnke, F.L. Martin, Ultrarapid On-Site detection of SARS-CoV-2 infection using simple ATR-FTIR spectroscopy and an analysis algorithm: high sensitivity and specificity, Anal. Chem. 93 (2021), https://doi.org/10.1021/acs.analchem.0c04608.
[62] B.R. Wood, K. Kochan, D.E. Bedolla, N. Salazar-Quiroz, S.L. Grimley, D. Perez-Guaita, M.J. Baker, J. Vongsvivut, M.J. Tobin, K.R. Bambery, D. Christensen, S. Pasricha, A.K. Eden, A. Mclean, S. Roy, J.A. Roberts, J. Druce, D.A. Williamson, J. McAuley, M. Catton, D.F.J. Purcell, D.I. Godfrey, P. Heraud, Infrared based saliva screening test for COVID-19, Angew. Chem. Int. Ed. 60 (2021), https://doi.org/10.1002/anie.202104453.
[63] A. Martinez-Cuazitl, G.J. Vazquez-Zapien, M. Sanchez-Brito, J.H. Limon-Pacheco, M. Guerrero-Ruiz, F. Garibay-Gonzalez, R.J. Delgado-Macuil, M.G.G. de Jesus, M. A. Corona-Perezgrovas, A. Pereyra-Talamantes, M.M. Mata-Miranda, ATR-FTIR spectrum analysis of saliva samples from COVID-19 positive patients, Sci. Rep. 11 (2021), https://doi.org/10.1038/s41598-021-99529-w.
[64] K. Naseer, S. Ali, J. Qazi, ATR-FTIR spectroscopy based differentiation of typhoid and dengue fever in infected human sera, Infrared Phys. Technol. 114 (2021), https://doi.org/10.1016/j.infrared.2021.103664.
[65] L. Dong, X. Duan, L. Bin, J. Wang, Q. Gao, X. Sun, Y. Xu, Evaluation of Fourier transform infrared (FTIR) spectroscopy with multivariate analysis as a novel diagnostic tool for lymph node metastasis in gastric cancer, Spectrochim. Acta Mol. Biomol. Spectrosc. 289 (2023), https://doi.org/10.1016/j.saa.2022.122209.
[66] Z. Guleken, A. Aday, A.G. Bayrak, İ.Y. Hindilerden, M. Nalçacı, J. Cebulski, J. Depciuch, Relationship between amide ratio assessed by Fourier-transform

infrared spectroscopy: a biomarker candidate for polycythemia vera disease, J. Biophot. (2024), https://doi.org/10.1002/jbio.202400162.
[67] J. Sajid, A. Elhaddaoui, S. Turrell, Fourier transform vibrational spectroscopic analysis of human cerebral tissue, J. Raman Spectrosc. 28 (1997) 2, https://doi.org/10.1002/(sici)1097-4555(199702)28:2/3<165::aid-jrs76>3.0.co.
[68] M. Szczerbowska-Boruchowska, P. Dumas, M.Z. Kastyak, J. Chwiej, M. Lankosz, D. Adamek, A. Krygowska-Wajs, Biomolecular investigation of human substantia nigra in Parkinson's disease by synchrotron radiation Fourier transform infrared microspectroscopy, Arch. Biochem. Biophys. 459 (2007) 241–248, https://doi.org/10.1016/J.ABB.2006.12.027.
[69] E.G. Ahmed, N.A. Al-Muslet, M.M. Ahmed, M.A. Moharam, W. Musaad, The use of fourier infrared spectroscopy and laser – raman spectroscopy in bladder malignancy diagnosis, A comparative Study, Appl. Phys. Res. 2 (2010), https://doi.org/10.5539/apr.v2n1p108.
[70] N. Fujioka, Y. Morimoto, T. Arai, K. Takeuchi, M. Yoshioka, M. Kikuchi, Differences between infrared spectra of normal and neoplastic human gastric cells, Spectroscopy 18 (2004) 59–66, https://doi.org/10.1155/2004/347480.
[71] V. Balan, C.T. Mihai, F.D. Cojocaru, C.M. Uritu, G. Dodi, D. Botezat, I. Gardikiotis, Vibrational spectroscopy fingerprinting in medicine: from molecular to clinical practice, Materials 12 (2019), https://doi.org/10.3390/ma12182884.
[72] C. Delrue, M. Hofmans, J. Van Dorpe, M. Van der Linden, Z. Van Gaever, T. Kerre, M.M. Speeckaert, S. De Bruyne, Innovative label-free lymphoma diagnosis using infrared spectroscopy and machine learning on tissue sections, Commun. Biol. 7 (2024) 1419, https://doi.org/10.1038/s42003-024-07111-7.
[73] A. Barth, Infrared spectroscopy of proteins, Biochim. Biophys. Acta Bioenerg. 1767 (2007) 1073–1101, https://doi.org/10.1016/J.BBABIO.2007.06.004.
[74] S.Y. Chun, M.K. Son, C.R. Park, C. Lim, H.I. Kim, K. Kwak, M. Cho, Direct observation of protein structural transitions through entire amyloid aggregation processes in water using 2D-IR spectroscopy, Chem. Sci. (2022), https://doi.org/10.1039/d1sc06047c.
[75] M. Verdonck, A. Denayer, B. Delvaux, S. Garaud, R. De Wind, C. Desmedt, C. Sotiriou, K. Willard-Gallo, E. Goormaghtigh, Characterization of human breast cancer tissues by infrared imaging, Analyst 141 (2016), https://doi.org/10.1039/c5an01512j.
[76] R. Eckel, H. Huo, H.W. Guan, X. Hu, X. Che, W.D. Huang, Characteristic infrared spectroscopic patterns in the protein bands of human breast cancer tissue, Vib. Spectrosc. 27 (2001), https://doi.org/10.1016/S0924-2031(01)00134-5.
[77] P.G.L. Andrus, R.D. Strickland, Cancer grading by Fourier transform infrared spectroscopy, Biospectroscopy 4, https://doi.org/10.1002/(SICI)1520-6343(1998)4:1<37::AID-BSPY4>3.0.CO, 1998.
[78] Y. Liu, Y. Xu, Y. Liu, Y. Zhang, D. Wang, D. Xiu, Z. Xu, X. Zhou, J. Wu, X. Ling, Detection of cervical metastatic lymph nodes in papillary thyroid carcinoma by Fourier transform infrared spectroscopy, Br. J. Surg. 98 (2011), https://doi.org/10.1002/bjs.7330.
[79] M.J. Baker, J. Trevisan, P. Bassan, R. Bhargava, H.J. Butler, K.M. Dorling, P. R. Fielden, S.W. Fogarty, N.J. Fullwood, K.A. Heys, C. Hughes, P. Lasch, P. L. Martin-Hirsch, B. Obinaju, G.D. Sockalingum, J. Sulé-Suso, R.J. Strong, M. J. Walsh, B.R. Wood, P. Gardner, F.L. Martin, Using Fourier transform IR spectroscopy to analyze biological materials, Nat. Protoc. 9 (2014) 1771–1791, https://doi.org/10.1038/nprot.2014.110.
[80] X. Wu, W. Shuai, C. Chen, X. Chen, C. Luo, Y. Chen, Y. Shi, Z. Li, X. Lv, C. Chen, X. Meng, X. Lei, L. Wu, Rapid screening for autoimmune diseases using Fourier transform infrared spectroscopy and deep learning algorithms, Front. Immunol. 14 (2023), https://doi.org/10.3389/fimmu.2023.1328228.
[81] W. Shuai, X. Wu, C. Chen, E. Zuo, X. Chen, Z. Li, X. Lv, L. Wu, C. Chen, Rapid diagnosis of rheumatoid arthritis and ankylosing spondylitis based on Fourier transform infrared spectroscopy and deep learning, Photodiagnosis Photodyn. Ther. 45 (2024), https://doi.org/10.1016/j.pdpdt.2023.103885.
[82] N. Zheng, T. Yang, M. Liang, H. Zhang, L. Li, A. Sunnassee, L. Liu, Characterization of protein in old myocardial infarction by FTIR micro-spectroscopy, J. Huazhong University Sci.Technol. Med.Sci. 30 (2010), https://doi.org/10.1007/s11596-010-0466-9.
[83] H.T. Teker, T. Ceylani, S. Keskin, G. Samgane, H. Allahverdi, E. Acikgoz, R. Gurbanov, Supplementing probiotics during intermittent fasting proves more effective in restoring ileum and colon tissues in aged rats, J. Cell Mol. Med. 28 (2024), https://doi.org/10.1111/jcmm.18203.
[84] C. Aksoy, F.A. Kaya, B.B. Kuşkonmaz, D. Uçkan, F. Severcan, Structural investigation of donor age effect on human bone marrow mesenchymal stem cells: FTIR spectroscopy and imaging, Age 36 (2014), https://doi.org/10.1007/s11357-014-9691-7.
[85] O. Calvo-Gomez, H. Calvo, L. Cedillo-Barrón, H. Vivanco-Cid, J.M. Alvarado-Orozco, D.A. Fernandez-Benavides, L. Arriaga-Pizano, E. Ferat-Osorio, J.C. Anda-Garay, C. López-Macias, M.G. López, Potential of ATR-FTIR-Chemometrics in Covid-19: disease recognition, ACS Omega 7 (2022), https://doi.org/10.1021/acsomega.2c01374.
[86] E. Roth, M. Bergmann, Importance of cytokine metabolism for malnutrition, catabolism and endocrinological state in sepsis, in: H. Redl, G. Schlag (Eds.), Cytokines in Severe Sepsis and Septic Shock, Birkhäuser Basel, Basel, 1999, pp. 227–243, https://doi.org/10.1007/978-3-0348-8755-7_13.
[87] T.G. Rocha, F.D.F. Silva, C. Bortoletto, D.G. Silva, M.G. Buzinaro, L.F. Zafalon, J. J. Fagliari, Serum concentrations of acute phase proteins and immunoglobulins of calves with rotavirus diarrhea, Arq. Bras. Med. Vet. Zootec. 68 (2016), https://doi.org/10.1590/1678-4162-7965.
[88] T.E. Andargie, K. Roznik, N. Redekar, T. Hill, W. Zhou, Z. Apalara, H. Kong, O. Gordon, R. Meda, W. Park, T.S. Johnston, Y. Wang, S. Brady, H. Ji, J. A. Yanovski, M.K. Jang, C.M. Lee, A.H. Karaba, A.L. Cox, S. Agbor-Enoh, Cell-free DNA reveals distinct pathology of multisystem inflammatory syndrome in children, J. Clin. Investig. 133 (2023), https://doi.org/10.1172/JCI171729.
[89] E. Stec-Martyna, K. Wojtczak, D. Nowak, R. Stawski, Battle of the biomarkers of systemic inflammation, Biology 14 (2025), https://doi.org/10.3390/biology14040438.
[90] T.J. Gould, Z. Lysov, P.C. Liaw, Extracellular DNA and histones: double-edged swords in immunothrombosis, J. Thromb. Haemostasis 13 (2015), https://doi.org/10.1111/jth.12977.
[91] H.M. Prosser, E.M. Bortoluzzi, R.J. Valeris-Chacin, E.C. Baker, M.A. Scott, Application of artificial intelligence and machine learning in bovine respiratory disease prevention, diagnosis, and classification, Am. J. Vet. Res. (2025) 1–5, https://doi.org/10.2460/ajvr.24.10.0327.
[92] A.A. AlZubi, Detection of disease in calves using artificial intelligence, Indian J. Anim. Res. (2024), https://doi.org/10.18805/ijar.bf-1760.
[93] M. Taneja, J. Byabazaire, N. Jalodia, A. Davy, C. Olariu, P. Malone, Machine learning based fog computing assisted data-driven approach for early lameness detection in dairy cattle, Comput. Electron. Agric. 171 (2020), https://doi.org/10.1016/j.compag.2020.105286.
[94] P. Swapna, M. Geetha, B. Nuthana, R. Rohan, Using AI and machine learning for early detection and management of cattle diseases to improve livestock health and productivity, Int. Res. J. Edu. Technol. Peer Rev.J. 6 (2024) 1815–1822.
[95] Y. Wang, Q. Li, M. Chu, X. Kang, G. Liu, Application of infrared thermography and machine learning techniques in cattle health assessments: a review, Biosyst. Eng. 230 (2023), https://doi.org/10.1016/j.biosystemseng.2023.05.002.
[96] C. Senthilkumar, S. C, G. Vadivu, S. Neethirajan, Early detection of lumpy skin disease in cattle using deep learning—A comparative analysis of pretrained models, Vet. Sci. 11 (2024), https://doi.org/10.3390/vetsci11100510.
[97] C. Piras, O.J. Hale, C.K. Reynolds, A.K. (Barney) Jones, N. Taylor, M. Morris, R. Cramer, LAP-MALDI MS coupled with machine learning: an ambient mass spectrometry approach for high-throughput diagnostics, Chem. Sci. 13 (2022), https://doi.org/10.1039/d1sc05171g.